ACS APPLIED MATERIALS & INTERFACES

Research Article

www.acsami.org

Efficient Low-Temperature Transparent Electrocatalytic Layers Based on Graphene Oxide Nanosheets for Dye-Sensitized Solar Cells

Seon Hee Seo,*[,†] Eun Ji Jeong,[†,‡] Joong Tark Han,[†] Hyon Chol Kang,[‡] Seung I. Cha,[†] Dong Yoon Lee,[†] and Geon-Woong Lee[†]

[†]Nano Hybrid Technology Research Center, Korea Electrotechnology Research Institute, Changwon 641-120, Korea

[‡]Department of Advanced Materials Engineering, College of Engineering, Chosun University, Gwangju 501-759, Korea

Supporting Information

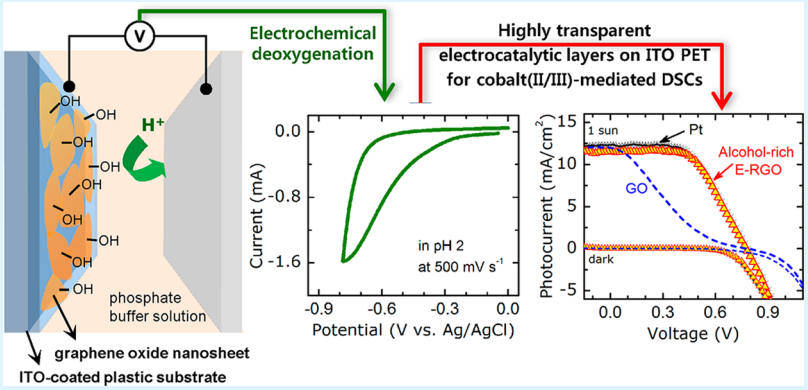

ABSTRACT: Electrocatalytic materials with a porous structure have been fabricated on glass substrates, via high-temperature fabrication, for application as alternatives to platinum in dye-sensitized solar cells (DSCs). Efficient, nonporous, nanometer-thick electrocatalytic layers based on graphene oxide (GO) nanosheets were prepared on plastic substrates using electrochemical control at low temperatures of ≤100 °C. Single-layer, oxygen-rich GO nanosheets prepared on indium tin oxide (ITO) substrates were electrochemically deoxygenated in acidic medium within a narrow scan range in order to obtain marginally reduced GO at minimum expense of the oxygen groups. The resulting electrochemically reduced GO (E-RGO) had a high density of residual alcohol groups with high electrocatalytic activity toward the positively charged cobalt-complex redox mediators used in DSCs. The ultrathin, alcohol-rich E-RGO layer on ITO-coated poly(ethylene terephthalate) was successfully applied as a lightweight, low-temperature counter electrode with an extremely high optical transmittance of ~97.7% at 550 nm. A cobalt(II/III)-mediated DSC employing the highly transparent, alcohol-rich E-RGO electrode exhibited a photovoltaic power conversion efficiency of 5.07%. This is superior to that obtained with conventionally reduced GO using hydrazine (3.94%) and even similar to that obtained with platinum (5.10%). This is the first report of a highly transparent planar electrocatalytic layer based on carbonaceous materials fabricated on ITO plastics for application in DSCs.

KEYWORDS: *graphene oxide, electrocatalyst, low-temperature fabrication, transparent counter electrode, dye-sensitized solar cell*

INTRODUCTION

Dye-sensitized solar cells (DSCs) have been intensively studied as promising alternatives to inorganic solar cells for low-cost power generation.[1,2] DSCs offer advantages such as insensitivity to the incidence angle of irradiated light, high transparency, and cost-effective manufacturing with nanomaterials; these features allow for unique applications of transparent building-integrated photovoltaics (BIPVs) and lightweight portable power sources with short energy payback.[3,4] DSCs typically consist of a mesoporous TiO_2 photoanode coated with light-absorbing molecules and a counter electrode (CE) separated by an organic electrolyte layer. Redox mediators dissolved in the electrolyte shuttle charge from the CE to the oxidized photoanode. The CE should efficiently transfer charge to the oxidized redox mediator at the CE/electrolyte interface. The transparency of CEs is critical for developing transparent BIPVs and high-performance flexible DSCs that are constructed on metal foils as nontransparent photoanodes that are inevitably irradiated from the side of the transparent CE.

A platinized F-doped SnO_2 (FTO) glass with a high optical transmittance of >90% at a wavelength of 550 nm ($\%T_{550nm}$) is conventionally used as a CE after sintering a platinum precursor at ~400 °C.[5,6] For the cost-effective fabrication of lightweight DSCs, there is a strong demand to replace platinum with low-cost materials fabricated on plastic substrates through low-temperature techniques. Most studies on platinum-free CEs

Received: March 4, 2015
Accepted: May 6, 2015
Published: May 6, 2015

DOI: 10.1021/acsami.5b01938
ACS Appl. Mater. Interfaces 2015, 7, 10863−10871

have focused on porous alternative materials, such as inorganic compounds,[7] conducting polymers,[8−10] and carbonaceous materials,[11−13] with high specific surface areas generated on glass substrates for high-performance DSC applications employing a conventional iodide/tri-iodide (I^-/I_3^-) redox electrolyte. Notably, the remarkable electrochemical performance of these porous CEs has been achieved by generating large surface areas rather than by increasing the charge-transfer rate at the corresponding interface.

Recently, it was reported that transparent nanocarbon-based CEs ($\%T_{550nm}$ > 85%) may be more effective in outer-sphere cobalt-complex redox mediators,[14,15] such as cobalt(II/III)tris-(2,2′-bipyridine) ($Co(bpy)_3^{2+/3+}$), than in the I^-/I_3^- redox electrolyte. We also reported that chemically assembled ultrashort carbon nanotube arrays with carboxyl termination on FTO glass exhibited markedly improved electrocatalytic activity toward positively charged $Co(bpy)_3^{2+/3+}$ redox mediators as compared to negatively charged I^-/I_3^-,[16] which suggested that the electrostatic attraction may play an important role in accelerating charge transfer at the CE/electrolyte interface.[17,18]

Irrespective of the thickness of the electrocatalytic layers and the type of redox mediators used in DSCs, most nanocarbon-based CEs, including graphene nanoplatelets (GNPs),[12,19,20] reduced graphene oxides (RGO) nanosheets,[14,17,21,22] and carbon nanotubes,[11,16,23] must be thermally activated above 300 °C to obtain high electrocatalytic activities. Such high temperatures hinder the application of these nanocarbon materials to CEs on plastic substrates. Consequently, transparent CEs on plastics have generally been prepared by using conducting polymers[24,25] and platinum.[26−28] However, these flexible polymer-based porous CEs had unique colors and relatively low transparency ($\%T_{550nm}$ < 70%); furthermore, low-temperature transparent platinum CEs undesirably promulgate the use of expensive noble metals.

To fabricate cost-effective transparent CEs, single-layer graphene oxide (GO) nanosheets are promising candidates among nanocarbon materials because they are rich in oxygen-containing functional groups, such as epoxide, carbonyl, hydroxyl, and carboxyl moieties.[29,30] The hydrophilicity of these oxygen groups permits facile coating of GO nanosheets in a two-dimensional layer on hydrophilic conducting substrates. For practical applications, insulating oxygen-rich GO has been converted into conducting oxygen-less RGO by using reduction methods that generally utilize hazardous chemicals ($NaBH_4$ and N_2H_4) and/or at high temperatures (>700 °C) in an inert atmosphere.[31−33] To date, most reduction methods have pursued complete removal of oxygen to achieve high electrical conductivity by reconstructing the graphitic sp^2 structure, and the atomic ratio of carbon to oxygen (C/O) has been widely adopted as an indicator of the degree of recovery of the graphene structure, ignoring the kinds of residual oxygen groups. However, from electrochemical perspective, carbon surface defects terminated by carboxyl and hydroxyl groups are considered to be more active than the sp^2 basal planes.[34] This implies that excessive removal of the electro-active oxygen groups degrades the electrochemical performance of RGO. Therefore, the number of effective oxygen groups remaining should be controlled as a factor influencing the electrocatalytic performance, but this aspect has barely been considered.

Herein, we present electrochemical control of residual oxygen groups in atomically thin GO layers prepared on indium tin oxide (ITO)-coated substrates for efficient low-temperature transparent CEs by using an electrochemical deoxygenation method. Nonporous, planar, oxygen-rich GO layers are marginally reduced in acidic phosphate buffer solution (PBS) within a narrow scan range at minimum expense of alcohol groups. The electrochemically reduced GO (E-RGO) with a high density of residual alcohol groups on ITO-coated poly(ethylene terephthalate) (ITO PET) is applied as a lightweight low-temperature transparent CE ($\%T_{550nm}$ > 97%) in $Co(bpy)_3^{2+/3+}$-mediated DSCs for the first time, to the best of our knowledge.[35] The high density of negatively charged alcohol groups remaining in the nanometer-thick E-RGO layer with minimal graphitization facilitated the charge transfer toward positively charged $Co(bpy)_3^{2+/3+}$ redox mediators at the E-RGO/electrolyte interface.

EXPERIMENTAL SECTION

Preparation of GO-Coated Electrodes. Graphite oxide powder was produced by using a modified Hummers method from natural graphite (Alfa Aesar, 99.999% purity −200mesh). Details are explained in elsewhere.[36] The resultant graphite oxide powder was dissolved in water to a concentration of 1 g L^{-1} and the resultant solution was sonicated for 1 h to exfoliate into GO nanosheets. For spin-coating of GO nanosheets, the solution was diluted into 40 mg L^{-1}. All substrates used were exposed to ultraviolet/O_3 for 20 min to obtain hydrophilic surfaces. GO nanosheets were deposited by successive 2 mL drops of the prepared dilute GO solution on the pretreated substrates spinning at 1000 rpm for 5 min under N_2 blowing. Films were dried in an oven at 100 °C for 2 h. For electrochemical deoxygenation, GO-coated electrodes were immersed in a three-electrode cell with N_2-purged 0.05 M PBS (Aldrich) and potential scans were performed by using a potentiostat (BioLogic SP-300). A silver/silver chloride (Ag/AgCl) wire in sealed NaCl (3 M) served as the reference electrode (BAS) in conjunction with a Pt auxiliary electrode (plate, 3 × 3 cm^2). The pH values of PBS were adjusted with HNO_3 and KOH. For chemical reduction, GO-coated electrodes were placed in a cleaned Petri dish inside a larger glass Petri dish with 1 mL of hydrazine monohydrate (98%, Aldrich). The container was placed over a hot plate at 100 °C for 15 h.

Preparation of Chemically Converted Pt Electrode. Chloroplatinic acid hydrate ($H_2PtCl_6{\cdot}6H_2O$, Aldrich, 0.1036 g) was dissolved in 5 mL of a mixture solvent (2-propanol/water = 8:2, v/v), followed by the addition of 10 drops of 10 mM $NaBH_4$ ethanol solution (0.0378 g of $NaBH_4$ in 100 mL of ethanol). The precursor solution was immediately hand-sprayed on ITO PET at 100 °C and the resultant electrodes were dried in an oven at 100 °C for 1 h. The dried light-yellow precursor electrodes were subsequently immersed in a reducing agent solution of 10 mM $NaBH_4$ stored in a freezer. The resultant chemically converted Pt (C-Pt) electrodes were washed with ethanol and water.

Fabrication of Cobalt(II/III)-Mediated DSCs. Mesoporous TiO_2 layers were prepared on FTO glasses (15 Ω sq^{-1}, Hartford) by using a screen-printing method and applied as photoanodes for DSCs as mentioned in reference.[16] The TiO_2 photoanodes were immersed in an alkyl-functionalized carbazol MK-2 dye solution (0.3 mM in dry toluene, Aldrich) for 15 h. The stained TiO_2 electrodes were assembled with the prepared GO-based or C-Pt electrodes along with a 25 μm-thick Surlyn gasket (Meltronix 1170−25, Solaronix). The composition of the electrolyte was 0.165 M $[Co(bpy)_3](PF_6)_2$, 0.045 M $[Co(bpy)_3](PF_6)_3$, 0.1 M $LiClO_4$ (Aldrich), and 0.2 M 4-*tert*-butylpyridine (Aldrich) in acetonitrile. The $Co(bpy)_3^{2+/3+}$ redox mediators ($[Co(bpy)_3](PF_6)_2$ and its oxidized form $[Co(bpy)_3](PF_6)_3$) were synthesized as reported previously.[18]

Characterization and Measurements. Atomic force microscopy (AFM) height images were obtained by XE-100 (Park System). The top-view images of the as-prepared GO and the chemically converted Pt were obtained by scanning electron microscopy (SEM, Hitachi S4800). Ultraviolet−visible (UV−vis) spectroscopy was performed using a Carry 5000 spectrophotometer (Varian). For measurements of

DOI: 10.1021/acsami.5b01938
ACS Appl. Mater. Interfaces 2015, 7, 10863−10871

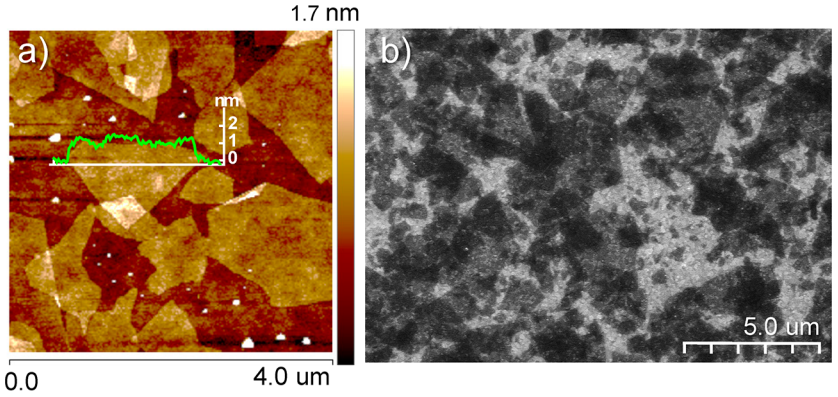

Figure 1. (a) An AFM image and corresponding height profile of GO coated on a SiO_2/Si wafer and (b) a top-view SEM image of GO coated on ITO glass.

X-ray photoelectron spectroscopy (XPS) and attenuated total reflectance Fourier transformation infrared (ATR-FTIR), relatively thick GO films were prepared by using a commercial automatic spray coater (NCS-400 with a 1.2 mm nozzle diameter) with a thick aqueous GO solution (1 g L^{-1}) on Au-coated Si wafer and ITO glass, respectively. The amount of coated GO was fixed with respect to the number of spraying counts at 60 (distance between the nozzle and the substrate 70 mm, feeding rate 1 mL min^{-1}, speed 400 mm s^{-1}). ATR-FTIR spectra were recorded on a Jasco FT/IR-4200 spectrometer with a commercial ATR accessory. XPS spectra were measured by using focused monochromatized Al Kα radiation in diameter of 400 μm (K-Alpha, Thermo Scientific).

For electrochemical characterization, cyclic voltammetry (CV) was performed in a three-electrode setup using a BioLogic SP-300 potentiostat. The electrolyte used was an acetonitrile solution containing 2 mM $[Co(bpy)_3](PF_6)_2$ and 0.1 M tetrabutylammonium hexafluorophosphate (TBA·PF_6). A Pt plate and a Ag/Ag^+ reference electrode (10 mM $AgNO_3$ and 0.1 M TBA·PF_6 in acetonitrile) were used as the counter and the reference electrodes, respectively. The photocurrent–voltage (J–V) characteristics were determined using a Keithley model 2400 source measurement unit. The irradiation source was a 300 W xenon lamp on an Oriel solar simulator with an air mass 1.5G filter. To eliminate the diffuse scattering from the edges of the glass substrates during the photovoltaic J–V measurements, black masks were attached on the surfaces of the DSCs, and the active area was defined to 0.1963 cm^2. Electrochemical impedance spectroscopy (EIS) was performed with DSCs used in measurements of photovoltaic J–V curves under the simulated light of 100 mW cm^{-2} at open-circuit conditions. The modulation amplitude was 10 mV and the frequency range was 0.3 Hz to 200 kHz. The EIS data were processed using EC-Lab software.

RESULTS AND DISCUSSION

To form a two-dimensional, atomically thin GO layer, GO was spin-coated on ultraviolet/O_3-treated hydrophilic ITO-coated substrates by addition of successive 2 mL drops of a 40 mg L^{-1} GO solution under N_2 blowing. To investigate the surface morphology and dimensions of the GO coating, the AFM image of a GO-coated SiO_2/Si sample (Figure 1a) was acquired. The GO coating sheets had a wide size distribution from ~2 μm and a height of ~1.5 nm. The spin-coating method provided an atomically planar surface of single-layer GO with partial coverage of the substrate,[33] similar to the case of spin coating on polycrystalline ITO glass (Figure 1b). Optical transmittance of the nanometer-thick GO layer was ~99.3% at 550 nm ($\%T_{550nm}$, see Figure S1 in the Supporting Information), indicating extremely low loading of the GO nanosheets.

The nanometer-thick GO layers were electrochemically deoxygenated by means of CV in PBS. During the potential scan in the negative direction, the deoxygenation of oxygen-containing functional groups in GO occurred irreversibly in the presence of proton in the PBS,[37] and a resulting cathodic peak was apparent below −0.8 V depending on the scan rate and the pH of the PBS electrolyte. In electrochemistry, the pH of an electrolyte critically affects the charge-transfer kinetics at an electrode/electrolyte interface.[38] Despite this fact, there are few detailed studies treating the effect of pH on the electrochemical properties of E-RGO electrodes.[17,37,39−41] To fill this gap, herein, the potential was cycled between 0 V and a lower limit in PBS electrolytes with different pH values at a scan rate of 500 mV s^{-1} (Figure 2a). The lower limits for each scan cycle were adjusted so as to retain transparent, water-clear ITO color after performing ten scan cycles: −0.8 V for pH 2, −1.1 V for pH 7.4, and −1.3 V for pH 10 (Figure 2a). Overly wide scan ranges negatively affected the electrical conductivity and transmittance of the conducting ITO substrate. As shown in Figure 2a, increasing the pH caused a shift of the cathodic peak potential toward lower potentials. This indicates that protons were actively involved as a reducing agent in deoxygenation of the GO electrode.[37]

The electrochemical performance of the E-RGO electrodes prepared under different conditions was studied by using CV in a three-electrode configuration with an organic dilute electrolyte containing a redox mediator used in DSCs. Figure 2b shows the CV curves obtained for 2 mM $Co(bpy)_3(PF_6)_2$ in acetonitrile acquired at a scan rate of 100 mV s^{-1}. In DSCs, the CE catalyzes the reversible reduction of the oxidized redox mediator ($Co(bpy)_3^{3+}$) and provides a reduced form of the redox mediator ($Co(bpy)_3^{2+}$). Therefore, under a given set of measurement conditions, the enhanced electrochemical performance may be evidenced by a higher cathodic peak current ($I_{p,c}$, proportional to the electro-active area) and smaller peak-to-peak separation potential (ΔE_p, inversely dependent on the charge-transfer rate at the corresponding interface).[42] A bare ITO substrate gave rise to an asymmetric curve with a substantially large ΔE_p, indicating poor electrochemistry on the ITO surface.

Coating the ITO substrate with a nanometer-thick GO layer and subsequent electrochemical deoxygenation of GO improved the electrochemical performances as indicated by the larger $I_{p,c}$ and decreased ΔE_p (Figure 2b). The apparent ΔE_p changed from 220 for as-prepared GO to 131 mV for E-RGO converted in basic PBS (pH 10). Moreover, an acidic

DOI: 10.1021/acsami.5b01938
ACS Appl. Mater. Interfaces 2015, 7, 10863−10871

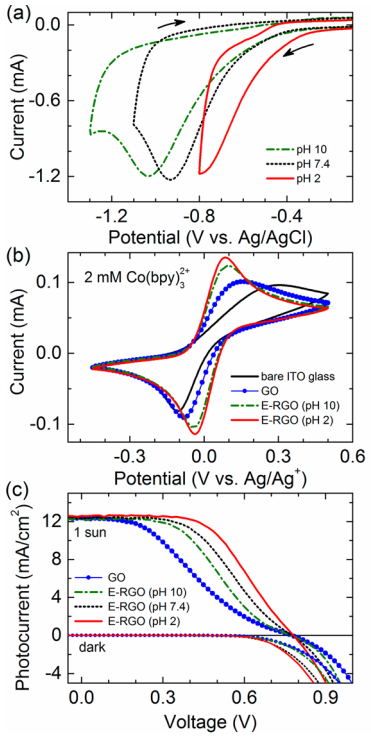

Figure 2. (a) CV curves for electrochemical deoxygenation of nanometer-thick GO layers in PBS with different pH values at a scan rate of 500 mV s^{-1}. (b) CV curves of GO-based electrodes in a three-electrode configuration in acetonitrile with 2 mM Co(bpy)$_3$(PF$_6$)$_2$ acquired at a scan rate of 100 mV s^{-1}. (c) Photovoltaic $J-V$ curves of Co(bpy)$_3^{2+/3+}$-mediated DSCs employing different E-RGO CEs under simulated light (100 mW cm^{-2}, 1 sun) and in the dark.

conversion environment further improved the electrocatalytic performance of E-RGO, as verified by the decrease of ΔE_p to 121 mV and the increase of the $I_{p,c}$. After ten successive scan cycles in the dilute Co(bpy)$_3^{2+/3+}$ redox electrolyte, there were no peak shifts or current reduction in the CV curves (Supporting Information Figure S2). This indicated that stable, quasi-reversible electrochemistry occurred on the E-RGO electrode prepared in acidic PBS (pH 2) for the Co(bpy)$_3^{2+/3+}$ redox reaction.

To examine the feasibility of using E-RGO as an electrocatalytic layer and to compare the electrochemical performance of the E-RGO electrodes prepared under different conditions, the different E-RGO electrodes on ITO glass substrates were utilized as the CE in Co(bpy)$_3^{2+/3+}$-mediated DSCs. Figure 2c shows representative photovoltaic $J-V$ curves under simulated AM 1.5G (100 mW cm^{-2}, 1 sun) irradiation and in the dark. The power conversion efficiency (η) of a solar cell is defined as the ratio of the maximum power ($J_m \times V_m$) determined from the measured $J-V$ curve to the irradiated incident light power, P_{inc} (100 mW cm^{-2} in this study). The electrochemical performance of the CE mainly affects the fill factor (FF)[11,43] corresponding to the "squareness" of the $J-V$ curve, defined by $(J_m \times V_m)/(J_{SC} \times V_{OC})$, where J_{SC} is the short-circuit current at $V = 0$ and V_{OC} is the open-circuit voltage at net zero current. The photovoltaic parameters are listed in Table 1. In this study, a commercial MK-2 organic dye was used as a readily accessible system for investigating the performance of the components used in Co(bpy)$_3^{2+/3+}$-mediated DSCs with an η of 5.5−6.5%[44] because using a commercial MK-2 organic dye facilitated use of a commercial TiO_2 paste for an efficient MK-2 sensitized mesoporous TiO_2 layer.

Table 1. Photovoltaic Parameters of Co(bpy)$_3^{2+/3+}$-Mediated DSCs Employing the GO-Based CEs on ITO Glass

CE	pH	J_{SC} (mA cm^{-2})	V_{OC} (V)	FF	η_{avg} (%)
GO		12.3	0.774	0.311	2.96 (±0.11)
E-RGO	10.0	12.2	0.771	0.435	4.11 (±0.32)
E-RGO	7.4	12.4	0.775	0.478	4.60 (±0.16)
E-RGO	2.0	12.6	0.781	0.543	5.34 (±0.03)

Improved photovoltaic performance can be easily recognized based on the larger second quarter area in the photovoltaic $J-V$ curves. The value of η increased from 2.96% for DSCs employing as-prepared GO to 5.34% for those employing E-RGO (pH 2) CEs (Figure 2c and Supporting Information Figure S3). Decreasing the pH for electrochemical deoxygenation resulted in an increase of the FF from 0.435 to 0.543 due to enhanced electrochemical performance of the CE as explained in relation to Figure 2b. $J-V$ curves that are S-shaped near V_{OC} are frequently observed for DSCs employing transparent carbonaceous CEs,[16,19,45] and the S-shape was straightened out by increasing loading for a larger electro-active area.[45] Remarkably, using the proper conditions for electrochemical deoxygenation of the nanometer-thick GO layers changed the S-shape of the $J-V$ curves to the conventional profiles (Figure 2c), even though the physical surface area of the coated GO was not changed. This implies that the chemical evolution during the electrochemical deoxygenation process significantly affected the electrocatalytic activity of the GO-based electrodes.

Chemical Characterization of E-RGO Electrodes. The effect of the chemical parameters of the E-RGO electrodes on the electrochemical performance was evaluated based on chemical characterization of the GO samples prepared by using an automatic spray coater with subsequent electrochemical deoxygenation. The elemental composition of the GO and E-RGO films was confirmed from the XPS spectra. The degree of deoxygenation, represented by the atomic weight ratio of carbon to oxygen (C/O), was estimated by analysis of the XPS survey data, where C 1s and O 1s peaks were apparent at approximately 285 and 533 eV, respectively (Supporting Information Figure S4). The estimated C/O ratios are listed in Supporting Information Table S1. The initial C/O ratio of the as-prepared GO layer was ~2.8 and the ratio increased to ~4.2 after a single potential scan cycle, irrespective of the pH, in direct contrast with the electrochemical performance of the E-RGO electrodes prepared at pH 2 and pH 10 (Figures 2b−c). Increasing the number of scan cycles up to 50 at pH 2 increased the C/O ratio to ~6.8. The residual oxygen content of E-RGO could be controlled based on the number of scan cycles rather than by the pH. The optimal electrochemical performance was achieved with E-RGO subjected to deoxygenation conditions after a single potential scan within a narrow scan range in pH 2 PBS at a scan rate of 500 mV s^{-1}, denoted E-RGO (pH 2, 1), and the performance deteriorated with increasing numbers of scan cycles at pH 2 (Supporting Information Figures S5−S6). The evolution of the C/O ratios exactly followed the trend for the optical properties shown in Supporting Information Figure S7,[46] thus confirming that the extent of deoxygenation in the nanometer-thick E-RGO layer was not directly correlated to the overall electrocatalytic performance at the E-RGO/electrolyte interface.

DOI: 10.1021/acsami.5b01938
ACS Appl. Mater. Interfaces 2015, 7, 10863−10871

The statistical chemical states around the carbon atoms were evaluated by deconvolution of the C 1s region into four components;[31,47] sp^2 C═C at 284.5 eV, sp^3 C−C/C−H at ∼285.5 eV, C−O/C−O−C at ∼286.7 eV, and C═O/O−C═O at ∼288.2 eV, as shown by the dashed lines of the component fits in Figure 3a. The detailed deconvolution results

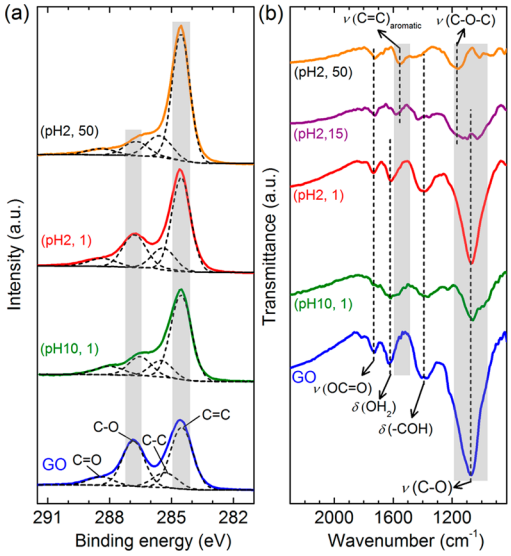

Figure 3. (a) C 1s region of XPS and (b) ATR-FTIR spectra of as-prepared GO and different E-RGO electrodes. E-RGO layers are denoted by the different experimental conditions (the pH of PBS, the number of scan cycles).

are summarized in Supporting Information Table S1. As electrochemical deoxygenation progressed, the intensity of the peaks of the sp^2 carbons (C═C) increased and deoxygenation occurred mainly at the C−O containing groups as C−OH or C−O−C (respective shaded regions in Figure 3a). The residual oxygen functionalities were also identified via ATR-FTIR spectroscopy. The ATR-FTIR spectrum of as-prepared GO was typified by four characteristic absorption bands at 1730, 1620, 1390, and 1070 cm^{-1}, assigned to the C═O stretching vibration of carboxyls, adsorbed water molecules, C−OH deformation, and C−O stretching of ethers, epoxides, and hydroxyls, respectively, which is consistent with previous results of GO[31,32,48] (Figure 3b and Supporting Information Figure S8).

The absorption intensity of the ν(C−O) band of E-RGO (pH 2, 1) decreased slightly compared to that of as-prepared GO, and gradually disappeared after 50 scan cycles, as shown in Figure 3b. Carboxyl and C−O−C groups were still present in the E-RGO (pH 2, 50) sample. Guo et al. suggested that deoxygenation of the C−O−C groups of GO required more negative potentials (−1.5 V),[39] and that the carboxyl and C−O−C groups were hardly removed during deoxygenation within a narrow scan range. The restoration of the hydrophobic graphitic sp^2 structure as a function of the number of scan cycles was evidenced by the disappearance of the water absorption peak at 1620 cm^{-1} and the appearance of the aromatic C═C mode at 1570 cm^{-1}.[31] However, the IR spectrum of the E-RGO (pH 10, 1) sample was obviously different with noticeably decreased intensity of the C−O vibration and broadened absorption near 1730 cm^{-1} even with the use of a single potential scan. During the electrochemical deoxygenation process, the $C-O^-$ groups deprotonated at pH 10 were preferentially deoxygenated in just a single potential cycle. However, the C−OH groups protonated at pH 2 were gradually removed with increasing numbers of scan cycles. Based on the XPS and ATR-FTIR spectra shown Figure 3, the as-prepared GO film was rich in alcohol (C−OH), and electrochemical deoxygenation mainly affected the number of the alcohol groups remaining. The high electrocatalytic activity of the alcohol-rich ultrathin E-RGO (pH 2, 1) electrode in the $Co(bpy)_3^{2+/3+}$ redox reaction may originate from the high density of alcohol groups remaining after minimal graphitization, in contrast with the low electrochemical activity of the alcohol-poor E-RGO (pH 10, 1) electrode, even with similarly low graphitization.

There are still arguments about which sites are more electroactive among the various structural defects terminated by oxygen, hydrogen, or dangling bonds.[35] A conclusive decision cannot be made based on the results presented in this study; however, it is obvious that the negatively charged surface of the nanocarbon electrodes was less amenable toward the negatively charged I^-/I_3^- redox mediators incorporating a slow two-electron redox reaction.[16,17] Xu et al. developed efficient, thin electrocatalytic multilayers on ITO glass for I^-/I_3^--mediated DSCs that were prepared by alternating cationic insulating polymeric monolayers and anionic GO nanosheets.[17] The improved electrochemical performance of the multilayers was attributed to the decreased electrostatic repulsion between negatively charge GO^- and I_3^- because of electrostatic surface modification with the cationic polymer. We also reported that chemically assembled carbon nanotube arrays with negatively charged surface carboxyl groups exhibited poor electrochemical activity for negatively charged I^-/I_3^-, but exhibited greatly improved electrocatalytic activity toward positively charged $Co(bpy)_3^{2+/3+}$.[16]

In this study, we demonstrated that the number of residual alcohol groups, controlled by the electrochemical method employed, may play a decisive role in the electrocatalytic performance of nanometer-thick E-RGO layers. High electrocatalytic activity in the $Co(bpy)_3^{2+/3+}$ redox electrolyte may result from the high density of negatively charged alcohol groups remaining in the nanometer-thick E-RGO layers with minimal graphitization. The electrostatic attraction would accelerate charge transfer at the corresponding interface,[18] identified with a blue-shift of the characteristic peak frequency (f_{max}) for charge transfer at the E-RGO/electrolyte interface estimated from EIS spectra, which is discussed in an ensuing section.

Alcohol-Rich E-RGO on ITO PET. To take advantage of the electrochemical deoxygenation method as a low-temperature fabrication technique, GO nanosheets were prepared on lightweight ITO PET (plastic) substrates. The ITO PET had sheet resistance (R_{sheet}) values ranging from 15 to 100 Ω sq^{-1} (%T_{550nm} ranging from 71.4% to 75.3% with respect to air as a basis, Supporting Information Figure S9), where the R_{sheet} value is one of the important factors affecting the η value of solar cells. GO layers spin-coated on ITO PET with different R_{sheet} values were electrochemically deoxygenated under the optimum deoxygenation conditions (i.e., pH 2, 1 cycle). CEs employing the resultant alcohol-rich E-RGO on ITO PET substrates were assembled with a TiO_2 photoanode on FTO glass and the photovoltaic $J-V$ curves were measured (Figure 4a). The photovoltaic parameters of the DSCs are summarized in Supporting Information Table S2. The variation in the R_{sheet} value of the ITO PET substrate induced a change in the slope

DOI: 10.1021/acsami.5b01938
ACS Appl. Mater. Interfaces 2015, 7, 10863−10871

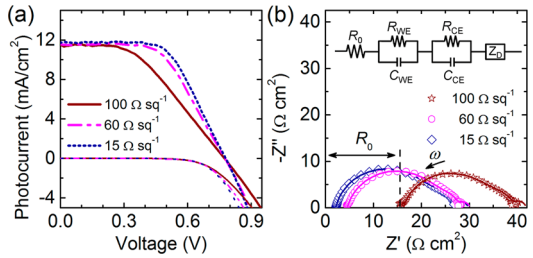

Figure 4. (a) Photovoltaic $J-V$ curves of $Co(bpy)_3^{2+/3+}$-mediated DSCs with CEs employing the alcohol-rich E-RGO on ITO PET substrates under simulated light (100 mW cm^{-2}, 1 sun) and in the dark. (b) The Nyquist plot of the EIS data for the DSCs under 1 sun illumination at open-circuit conditions. Solid lines are fitted results based on the equivalent circuit shown in the inset.

of the linear plots near V_{OC}; this linearity is quite different from the pronounced S-shaped curves in Figure 2c that were attributed to the low electrochemical performance of the CE. The decrease in the R_{sheet} value was associated with an increase of the FF from 0.441 to 0.596 and of η from 3.90% to 5.45%, indicating that the R_{sheet} value of conducting substrates for high-performance CEs should be lower than 60 Ω sq^{-1}. The highest value of η for the E-RGO on ITO PET was 5.45%, achieved using ITO PET with a low R_{sheet} value of 15 Ω sq^{-1}; this value was similar to that of E-RGO on ITO glass (5.34%) with a similar R_{sheet} value, as shown in Figure 2c.

To verify the effect of the R_{sheet} value of ITO PET-based CEs on the internal resistance of DSCs, EIS data were obtained for the DSCs under 1 sun illumination at open circuit conditions (Figure 4b). A well-established equivalent circuit consists of four components in series: an ohmic resistance (R_0), two reactive impedances from the photoanode (Z_{WE}) and the CE (Z_{CE}), and a Nernst diffusion impedance of the redox mediator within the electrolyte layer (Z_D) as shown in the inset of Figure 4b.[49−51] R_0 pertains to the intercept with the x-axis, and the reactive interfacial resistance at the electrode/electrolyte interface roughly corresponds to the diameter of the semicircle. The R_0 value generally depends on the R_{sheet} value of the electrodes and the contact resistance of the cell. A high-performance DSC generally gives rise to an impedance spectrum with three slightly overlapped, but distinct, semicircles offset from the origin along the x-axis in a Nyquist plot.[51]

In this study, the frequency-dependent impedances (Z_{WE}, Z_{CE}, and Z_D) were found to overlap considerably (Figure 4b). The overall shapes and sizes of the offset semicircles were mostly unaffected by the change of the ITO PET substrate with different R_{sheet} values, but the frequency-independent R_0 changed noticeably from 2.2 to 16.3 Ω cm^2 (Figure 4b). This strongly suggested that the η value of DSCs with alcohol-rich E-RGO on ITO PET is restricted mainly by the R_{sheet} value of the conducting ITO PET rather than by the electrochemical performance of the alcohol-rich E-RGO. Although the highest η value was achieved with the use of a highly conductive ITO PET substrate (15 Ω sq^{-1}), a moderately conductive ITO PET substrate (60 Ω sq^{-1}) was utilized for further investigations because of the low transmittance of the highly conductive ITO PET (Supporting Information Figure S9).

To confirm the competitiveness of alcohol-rich E-RGO as a low-temperature transparent electrocatalytic layer on ITO PET for efficient DSCs, other transparent CEs were also prepared with RGO and platinum through a chemical method compatible with plastic substrates. Spin-coated GO nanosheets (Figure 5a) and spray-coated platinum precursor layers on ITO

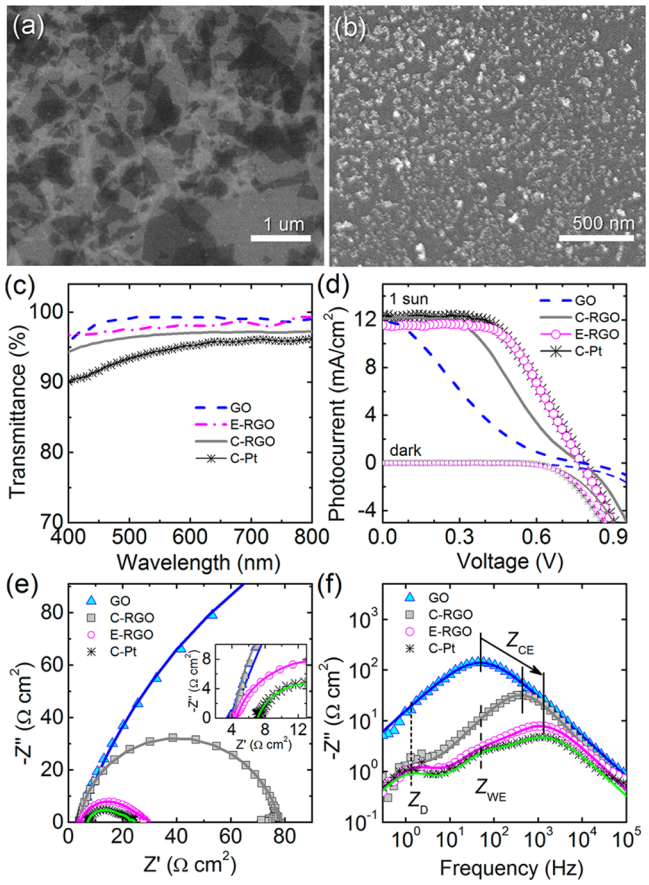

Figure 5. SEM images of (a) GO and (b) C-Pt on ITO PET. (c) Optical transmittances of the as-prepared GO, alcohol-rich E-RGO, C-RGO, and C-Pt layers with respect to ITO PET (60 Ω sq^{-1}) as a basis. (d) Photovoltaic $J-V$ curves of $Co(bpy)_3^{2+/3+}$-mediated DSCs employing different CEs on ITO PET. (e) The Nyquist plot and (f) imaginary impedances as a function of the frequency of the EIS data measured for the DSCs under 1 sun illumination at open-circuit conditions. Solid lines are fitted results based on the equivalent circuit, as shown in the inset of Figure 4b.

PET (60 Ω sq^{-1}) were chemically converted into RGO (C-RGO) and platinum nanoparticles (C-Pt, Figure 5b) using N_2H_4 and $NaBH_4$, respectively, as reducing agents. Figure 5c shows the optical transmittance of the as-prepared GO, alcohol-rich E-RGO, C-RGO, and C-Pt layers with respect to ITO PET as a basis. Electrochemical deoxygenation of GO resulted in a decrease of $\%T_{550nm}$ from 99.3% to 97.7% (Figure 5c). The conventional chemical reduction method using N_2H_4 vapor for C-RGO resulted in a lower transmittance of ∼96.7% because of a higher degree of sp^2 graphitization (Supporting Information Figure S10). The transmittance of C-Pt was adjusted to ∼94.4% by controlling the spraying time of the platinum precursor solution.

Figure 5d shows the photovoltaic $J-V$ curves of DSCs employing different CEs on ITO PET; the corresponding photovoltaic parameters are listed in Table 2. As-prepared GO exhibited very poor electrochemical performance, evidenced by the very pronounced S-shaped $J-V$ curve with a very low FF (0.201). The DSC assembled with the highly transparent alcohol-rich E-RGO CE exhibited good photovoltaic perform-

DOI: 10.1021/acsami.5b01938
ACS Appl. Mater. Interfaces 2015, 7, 10863−10871

Table 2. Photovoltaic and EIS parameters of $Co(bpy)_3^{2+/3+}$-Mediated DSCs with Different Low-Temperature Transparent CEs on ITO PET

CE	J_{SC} (mA cm^{-2})	V_{OC} (V)	FF	$\eta_{max/avg}$ (%)	R_0 (Ω cm^2)	R_{CE} (Ω cm^2)	C_{CE} (μF cm^{-2})	f_{max} (Hz)
GO	11.9	0.775	0.201	1.85/1.80 (±0.07)	4.1	383.0	8.6	48
C-RGO	12.1	0.775	0.420	3.94/3.83 (±0.08)	4.2	69.3	5.5	414
E-RGO	11.5	0.775	0.569	5.07/4.97 (±0.10)	4.6	19.3	6.8	1204
C-Pt	12.3	0.775	0.535	5.10/4.89 (±0.21)	7.1	12.2	10.0	1294

ance, with a FF of 0.569 and an η of 5.07%; these values are superior to those obtained using the highly graphitized C-RGO (FF = 0.420 and η = 3.94%) and were even similar to those achieved with the use of C-Pt (FF = 0.535 and η = 5.10%). The notable performance of the highly transparent nanometer-thick E-RGO CE is attributed to the high density of retained alcohol groups, as previously explained. Overall, the η values achieved in this study are lower than those of reported cobalt(II/III)-mediated DSCs with transparent CEs on FTO glass substrates,[14,15] however, judicious selection of the organic dyes accompanied by optimization of the TiO_2 photoanode should further enhance the photovoltaic performance of the cobalt(II/III)-mediated DSCs utilizing transparent alcohol-rich E-RGO CEs on plastic substrates.

Figures 5e–f show the Nyquist plot and the imaginary impedance as a function of the frequency of the EIS data measured for the DSCs under 1 sun illumination at open-circuit conditions. The effect of the constituent elements of the DSC on the photovoltaic performance can be estimated by fitting the EIS data based on the equivalent circuit, as shown in the inset of Figure 4b. Herein, since the assembly condition, the photoanode, the geometrical configuration, and the electrolyte for the DSCs were fixed, Z_{WE} and Z_D, shown in the mid- and low-frequency regions (10 Hz and <1 Hz), would be assumed to be marginally affected by the change of the CEs within experimental error. Therefore, focus was placed on the changes in R_0 and Z_{CE}, consisting of the charge-transfer resistance (R_{CE}) and the effective double-layer capacitance (C_{CE}). Details for fitting procedure are explained in elsewhere.[16] The fitting results are plotted as solid lines in Figures 5e–f and listed in Table 2 for R_0, R_{CE}, C_{CE}, and f_{max}, at which the absolute imaginary part of the impedance reaches its maximum in the Nyquist plot. The fitting results provide useful information on the interfacial charge-transfer reaction at the CE/electrolyte interface, such as the relative electro-active surface area, the charge-transfer rate, and the charge-transfer resistance.[50] C_{CE} is proportional to the effective surface area, and a change of C_{CE} indicates the relative variation of the electro-active surface areas. The product of R_{CE} and C_{CE} provides a time scale for the charge-transfer reaction, defined as a characteristic time constant or charge lifetime ($\tau_c = R_{CE}C_{CE} = 1/2\pi f_{max}$).[52] A blue-shift of f_{max} indicates a shorter lifetime due to faster charge transfer at the related interface.

The most noticeable feature of the EIS data for the GO-based electrodes was the decrease of the R_{CE} from 383.0 to 19.3 Ω cm^2, accompanied by the substantial shift of f_{max} from ~50 to ~1200 Hz, that is, toward a higher-frequency region, after the electrochemical deoxygenation (Figure 5f). A similar blue-shift of f_{max} was observed when the redox mediators were changed from I^-/I_3^- to $Co(bpy)_3^{2+/3+}$ in our previous study.[16] An increase of the effective surface area of the CEs would induce a decrease of R_{CE} and an increase of C_{CE} simultaneously, but would not account for the shift of f_{max} within experimental error. Because the charge-transfer rate depends on the composition of the electrolyte near the electrode and the nature and preparation of the interface,[52] f_{max} could be affected by the changes of electrical conductivity within the electrode or by the efficiency of charge transfer at the interface.

In general, deoxygenation of GO improves the electrical conductivity by healing damaged carbon structures. Although the alcohol-rich E-RGO might have a much low electrical conductivity than the more graphitized C-RGO, evidenced by the low C/O ratio of ~4.2 and the absence of the sp^2 C=C mode in the IR spectrum, the f_{max} value of alcohol-rich E-RGO (~1204 Hz) was higher than that of the more graphitized C-RGO (~48 Hz) and was even similar to that of C-Pt (~1294 Hz). This indicated that transfer of charge to the $Co(bpy)_3^{3+}$ redox mediator was faster at the alcohol-rich E-RGO/electrolyte interface. Moreover, the C_{CE} of alcohol-rich E-RGO (6.8 μF cm^{-2}) corresponded to 68% of that of the C-Pt (10.0 μF cm^{-2}), which indicates that the nonporous, atomically thin E-RGO layer had a smaller effective surface area than C-Pt (Figures 5a–b). The smaller R_{CE} value of C-Pt (12.2 Ω cm^2) relative to that of the alcohol-rich E-RGO (19.3 Ω cm^2) is attributed mainly to the larger effective surface area of the platinum nanoparticles. However, as shown in the inset of Figure 5e, the R_0 of C-Pt (7.1 Ω cm^2), which was larger than that of the other GO-based CEs (~4.3 Ω cm^2), might negatively affect the FF. The R_{sheet} value of ITO PET for C-Pt might be degraded during the chemical conversion in $NaBH_4$ solution. Therefore, the DSC employing C-Pt had an η value similar to that fabricated with the alcohol-rich E-RGO CE. This is the first report of the successful application of a highly transparent nanometer-thick electrocatalytic layer prepared on ITO-coated plastics at a low temperature for DSCs as far as we know.

CONCLUSION

In summary, efficient, nonporous, planar, atomically thin electrocatalytic layers based on GO nanosheets were prepared by using an electrochemical method compatible with plastic substrates. The number of alcohol groups (among various oxygen-containing functional groups) in the nanometer-thick GO layers on the ITO-coated substrates was mainly affected by the electrochemical deoxygenation conditions, including the pH of the buffer solution, the number of scan cycles, and the scan rate. The alcohol-rich E-RGO electrode prepared in acidic PBS (pH 2) presented higher electrocatalytic activity for the $Co(bpy)_3^{2+/3+}$ redox reaction than other alcohol-poor E-RGO electrodes, even with similarly low graphitization. The high electrocatalytic activity toward the $Co(bpy)_3^{2+/3+}$ redox reaction may result from improved electrostatic interaction between the positively charged $Co(bpy)_3^{2+/3+}$ redox mediators and the negatively charged alcohol groups remaining in the nanometer-thick E-RGO layers with minimal graphitization. The electrocatalytic performance of the alcohol-rich E-RGO electrode on ITO PET was superior to that of conventionally reduced GO employing N_2H_4 and was similar to that of platinum. The

DOI: 10.1021/acsami.5b01938
ACS Appl. Mater. Interfaces 2015, 7, 10863–10871

resultant E-RGO was successfully applied as a lightweight low-temperature transparent counter electrode ($\%T_{550nm}$ ~97.7%) in $Co(bpy)_3^{2+/3+}$-mediated DSCs, resulting in a power conversion efficiency of 5.07%, which is comparable to that of platinum (5.10%). This suggests that the highly electrocatalytic, ultrathin E-RGO layers are promising, low-cost substitutes for expensive platinum and other carbonaceous alternatives that requiring high energy-consuming processes for fabricating transparent CEs for use in transparent BIPV or metal-foil-based flexible DSCs.

■ ASSOCIATED CONTENT

Supporting Information

Optical transmittances, Raman spectra, CV curves of E-RGO, photographs of E-RGO, survey data and analysis results of XPS, ATR-FTIR spectra, and photovoltaic parameters of DSCs with alcohol-rich E-RGO on ITO PET. The Supporting Information is available free of charge on the ACS Publications website at DOI: 10.1021/acsami.5b01938.

■ AUTHOR INFORMATION

Corresponding Author

*E-mail: seosh@keri.re.kr.

Notes

The authors declare no competing financial interest.

■ ACKNOWLEDGMENTS

This work was supported by a grant from Korea Electrotechnology Research Institute (KERI).

■ REFERENCES

(1) O'Regan, B.; Grätzel, M. A Low-Cost, High-Efficiency Solar Cell Based on Dye-Sensitized Colloidal TiO_2 Films. *Nature* **1991**, *353*, 737−740.

(2) Hagfeldt, A.; Boschloo, G.; Sun, L.; Kloo, L.; Pettersson, H. Dye-Sensitized Solar Cells. *Chem. Rev.* **2010**, *110*, 6595−6663.

(3) Yoon, S.; Tak, S.; Kim, J.; Jun, Y.; Kang, K.; Park, J. Application of Transparent Dye-Sensitized Solar Cells to Building Integrated Photovoltaic Systems. *Build. Environ.* **2011**, *46*, 1899−1904.

(4) Ito, S.; Ha, N.-L. C.; Rothenberger, G.; Liska, P.; Comte, P.; Zakeeruddin, S. M.; Péchy, P.; Nazeeruddin, M. K.; Grätzel, M. High-Efficiency (7.2%) Flexible Dye-Sensitized Solar Cells with Ti-Metal Substrate for Nanocrystalline-TiO_2 Photoanode. *Chem. Commun.* **2006**, 4004−4006.

(5) Papgeorgiou, N. Counter-Electrode Function in Nanocrystalline Photoelectrochemical Cell Configurations. *Coord. Chem. Rev.* **2004**, *248*, 1421−1446.

(6) Seo, S. H.; Yoon, S. H.; Kim, M. H.; Jeong, E. J.; Kang, H. C.; Cha, S. I.; Lee, D. Y. Dependence of the Electrocatalytic Performance of Platinized Counter Electrodes on the Redox Mediator Employed in Dye-Sensitized Solar Cells. *J. Appl. Electrochem.* **2014**, *44*, 427−436.

(7) Thomas, S.; Deepak, T. G.; Anjusree, G. S.; Arun, T. A.; Nair, S. V.; Nair, A. S. A Review on Counter Electrode Materials in Dye-Sensitized Solar Cells. *J. Mater. Chem. A* **2014**, *2*, 4474−4490.

(8) Xia, J.; Chen, L.; Yanagida, S. Application of Polypyrrole as a Counter Electrode for a Dye-Sensitized Solar Cell. *J. Mater. Chem.* **2011**, *21*, 4644−4649.

(9) Tai, Q.; Chen, B.; Guo, F.; Xu, S.; Hu, H.; Sebo, B.; Zhao, X.-Z. In Situ Prepared Transparent Polyaniline Electrode and Its Application in Bifacial Dye-Sensitized Solar Cells. *ACS Nano* **2011**, *5*, 3795−3799.

(10) Yin, X.; Wu, F.; Fu, N.; Han, J.; Chen, D.; Xu, P.; He, M.; Lin, Y. Facile Synthesis of Poly(3,4-Ethylenedioxythiophene) Film via Solid-State Polymerization as High-Performance Pt-Free Counter Electrodes for Plastic Dye-Sensitized Solar Cells. *ACS Appl. Mater. Interfaces* **2013**, *5*, 8423−8429.

(11) Seo, S. H.; Kim, S. Y.; Koo, B.-K.; Cha, S. I.; Lee, D. Y. Influence of Electrolyte Composition on the Photovoltaic Performance and Stability of Dye-Sensitized Solar Cells with Multiwalled Carbon Nanotube Catalysts. *Langmuir* **2010**, *26*, 10341−10346.

(12) Roy-Mayhew, J. D.; Bozym, D. J.; Punckt, C.; Aksay, I. A. Functionalized Graphene as a Catalytic Counter Electrode in Dye-Sensitized Solar Cells. *ACS Nano* **2010**, *4*, 6203−6211.

(13) Wu, M.; Lin, X.; Wang, T.; Qiu, J.; Ma, T. Low-Cost Dye-Sensitized Solar Cell Based on Nine Kinds of Carbon Counter Electrodes. *Energy Environ. Sci.* **2011**, *4*, 2308−2315.

(14) Kavan, L.; Yum, J.-H.; Grätzel, M. Optically Transparent Cathode for Co(II/III) Mediated Dye-Sensitized Solar Cells Based on Graphene Oxide. *ACS Appl. Mater. Interfaces* **2012**, *4*, 6999−7006.

(15) Ju, M. J.; Jeon, I.-Y.; Kim, J. C.; Lim, K.; Choi, H.-J.; Jung, S.-M.; Choi, I. T.; Eom, Y. K.; Kwon, Y. J.; Ko, J.; Lee, J.-J.; Kim, H. K.; Baek, J.-B. Graphene Nanoplatelets Doped with N at its Edges as Metal-Free Cathodes for Organic Dye-Sensitized Solar Cells. *Adv. Mater.* **2014**, *26*, 3055−3062.

(16) Seo, S. H.; Kim, M. H.; Jeong, E. J.; Yoon, S. H.; Kang, H. C.; Cha, S. I.; Lee, D. Y. High Electrocatalytic Activity of Low-Loaded Transparent Carbon Nanotube Assemblies for $Co^{II/III}$-Mediated Dye-Sensitized Solar Cells. *J. Mater. Chem. A* **2014**, *2*, 2592−2598.

(17) Xu, X.; Huang, D.; Cao, K.; Wang, M.; Zakeeruddin, S. M.; Grätzel, M. Electrochemically Reduced Graphene Oxide Multilayer Films as Efficient Counter Electrode for Dye-Sensitized Solar Cells. *Sci. Rep.* **2013**, *1*, 1489.

(18) Feldt, S. M.; Gibson, E. A.; Gabrielsson, E.; Sun, L.; Boschloo, G.; Hagfeldt, A. Design of Organic Dyes and Cobalt Polypyridine Redox Mediators for High-Efficiency Dye-Sensitized Solar Cells. *J. Am. Chem. Soc.* **2010**, *132*, 16714−16724.

(19) Kavan, L.; Yum, J. H.; Grätzel, M. Optically Transparent Cathode for Dye-Sensitized Solar Cells Based on Graphene Nanoplatelets. *ACS Nano* **2011**, *5*, 165−172.

(20) Ju, M. J.; Jeon, I.-Y.; Lim, K.; Kim, J. C.; Choi, H.-J.; Choi, I. T.; Eom, Y. K.; Kwon, Y. J.; Ko, J.; Lee, J.-J.; Baek, J.-B.; Kim, H. K. Edge-Carboxylated Graphene Nanoplatelets as Oxygen-Rich Metal-Free Cathodes for Organic Dye-Sensitized Solar Cells. *Energy Environ. Sci.* **2014**, *7*, 1044−1052.

(21) Jang, H.-S.; Yun, J.-M.; Kim, D.-Y.; Park, D.-W.; Na, S.-I.; Kim, S.-S. Moderately Reduced Graphene Oxide as Transparent Counter Electrode for Dye-Sensitized Solar Cells. *Electrochim. Acta* **2012**, *81*, 301−307.

(22) Qiu, L.; Zhang, H.; Wang, W.; Chen, Y.; Wang, R. Effects of Hydrazine Hydrate Treatment on the Performance of Reduced Graphene Oxide Film as Counter Electrode in Dye-Sensitized Solar Cells. *Appl. Surf. Sci.* **2014**, *319*, 339−343.

(23) Cha, S. I.; Koo, B. K.; Seo, S. H.; Lee, D. Y. Pt-Free Transparent Counter Electrodes for Dye-Sensitized Solar Cells Prepared from Carbon Nanotube Micro-Balls. *J. Mater. Chem.* **2010**, *20*, 659−662.

(24) Idigoras, J.; Guillén, E.; Ramos, F. J.; Anta, J. A.; Nazeeruddin, M. K.; Ahmad, S. Highly Efficient Flexible Cathodes for Dye-Sensitized Solar Cells to Complement Pt@TCO Coating. *J. Mater. Chem. A* **2014**, *2*, 3175−3181.

(25) Lee, K. S.; Lee, Y.; Lee, J. Y.; Ahn, J.-H.; Park, J. H. Flexible and Platinum-Free Dye-Sensitized Solar Cells with Conducting-Polymer-Coated Graphene Counter Electrodes. *ChemSusChem* **2012**, *5*, 379−382.

(26) Dao, V.-D.; Nang, L. V.; Kim, E.-T.; Lee, J.-K.; Choi, H.-S. Pt Nanoparticles Immobilized on CVD-Grown Graphene as a Transparent Counter Electrode Material for Dye-Sensitized Solar Cells. *ChemSusChem* **2013**, *6*, 1316−1319.

(27) Fu, N.; Xio, X.; Zhou, X.; Zhang, J.; Lin, Y. Electrodeposition of Platinum on Plastic Substrates as Counter Electrodes for Flexible Dye-Sensitized Solar Cells. *J. Phys. Chem. C* **2012**, *4*, 2850−2857.

(28) Garcia-Alonso, D.; Zardetto, V.; Mackus, A. J. M.; Rossi, F. D.; Verheijen, M. A.; Brown, T. M.; Messels, W. M. M.; Creatore, M. Atomic Layer Deposition of Highly Transparent Platinum Counter Electrodes for Metal/Polymer Flexible Dye-Sensitized Solar Cells. *Adv. Energy Mater.* **2014**, DOI: 10.1002/aenm.201300831.

DOI: 10.1021/acsami.5b01938
ACS Appl. Mater. Interfaces 2015, 7, 10863−10871

(29) Lerf, A.; He, H.; Forster, M.; Klinowski, J. Structure of Graphite Oxide Revisited. *J. Phys. Chem. B* **1998**, *102*, 4477−4482.
(30) Chua, C. K.; Pumera, M. Chemical Reduction of Graphene Oxide: A Synthetic Chemistry Viewpoint. *Chem. Soc. Rev.* **2014**, *43*, 291−312.
(31) Zangmeister, C. D. Preparation and Evaluation of Graphite Oxide Reduced at 220 °C. *Chem. Mater.* **2010**, *22*, 5625−5629.
(32) Acik, M.; Lee, G.; Mattevi, C.; Chhowalla, M.; Cho, K.; Chabal, Y. J. Unusual Infrared-Absorbtion Mechanism in Thermally Reduced Graphene Oxide. *Nat. Mater.* **2010**, *9*, 840−845.
(33) Pei, S.; Cheng, H.-M. The Reduction of Graphene Oxide. *Carbon* **2012**, *50*, 3210−3228.
(34) McCreery, R. L. Advanced Carbon Electrode Materials for Molecular Electrochemistry. *Chem. Rev.* **2008**, *108*, 2646−2687.
(35) Kavan, L.; Yum, J. H.; Grätzel, M. Graphene-Based Cathodes for Liquid-Junction Dye-Sensitized Solar Cells: Electrocatalytic and Mass Transport Effects. *Electrochim. Acta* **2014**, *128*, 349−359.
(36) Lee, B. R.; Kim, J. S.; Nam, Y. S.; Jeong, H. J.; Jeong, S. Y.; Lee, G.-W.; Han, J. T.; Song, M. H. Highly Efficient Polymer Light-Emitting Diodes Using Graphene Oxide-Modified Flexible Single-Walled Carbon Nanotube Electrodes. *J. Mater. Chem.* **2012**, *22*, 21481−21486.
(37) Zhou, M.; Wang, Y.; Zhai, Y.; Zhai, J.; Ren, W.; Wang, F.; Dong, S. Controlled Synthesis of Large-Area and Patterned Electrochemically Reduced Graphene Oxide Films. *Chem.—Eur. J.* **2009**, *15*, 6116−6120.
(38) Garrett, D. J.; Flavel, B. S.; Shapter, J. G.; Baronian, K. H. R.; Downard, A. J. Robust Forests of Vertically Aligned Carbon Nanotubes Chemically Assembled on Carbon Substrates. *Langmuir* **2010**, *26*, 1848−1854.
(39) Guo, H.-L.; Wang, X.-F.; Qian, Q.-Y.; Wang, F.-B.; Xia, X.-H. A Green Approach to the Synthesis of Graphene Nanosheets. *ACS Nano* **2009**, *3*, 2653−2659.
(40) Raj, M. A.; John, S. A. Fabrication of Electrochemically Reduced Graphene Oxide Films on Glassy Carbon Electrode by Self-Assembly Method and Their Electrocatalytic Application. *J. Phys. Chem. C* **2013**, *117*, 4326−4335.
(41) Shao, Y.; Wang, J.; Engelhard, M.; Wang, C.; Lin, Y. Facile and Controllable Electrochemical Reduction of Graphene Oxide and Its Application. *J. Mater. Chem.* **2010**, *20*, 743−748.
(42) Bard, A. J.; Faulkner, L. R. *Electrochemical Methods: Fundamentals and Applications*, 2nd ed.; Wiley: New York, 2000; Chapter 6.
(43) Han, L.; Koide, N.; Chiba, Y.; Islan, A.; Komiya, R.; Fuke, N.; Fukui, A.; Yamanaka, R. Improvement of Efficiency of Dye-Sensitized Solar Cells by Reduction of Internal Resistance. *Appl. Phys. Lett.* **2005**, *86*, No. 213501.
(44) Murakami, T. N.; Koumura, N.; Uchiyama, T.; Uemura, Y.; Obuchi, K.; Masaki, N.; Kimura, M.; Mori, S. Recombination Inhibitive Structure of Organic Dyes for Cobalt Complex Redox Electrolytes in Dye-Sensitized Solar Cells. *J. Mater. Chem. A* **2013**, *1*, 792−798.
(45) Ramasamy, E.; Lee, W. J.; Lee, D. Y.; Song, J. S. Spray Coated Multi-Wall Carbon Nanotube Counter Electrode for Tri-iodide (I_3^-) Reduction in Dye-Sensitized Solar Cells. *Electrochem. Common.* **2008**, *10*, 1087−1089.
(46) Becerril, H. A.; Mao, J.; Liu, Z.; Stoltengerg, R. M.; Bao, Z.; Chen, Y. Evaluation of Solution-Processed Reduced Graphene Oxide Films as Transparent Conductors. *ACS Nano* **2008**, *2*, 463−470.
(47) Shin, H.-J.; Kim, K. K.; Benayad, A.; Yoon, S.-M.; Park, K.; Jung, I.-S.; Jin, M. H.; Jeong, H.-K.; Kim, J.-M.; Choi, J.-Y.; Lee, Y. H. Efficient Reduction of Graphite Oxide by Sodium Borohydride and Its Effect on Electrical Conductance. *Adv. Funct. Mater.* **2009**, *19*, 1987−1992.
(48) Szabó, T.; Berkesi, O.; Dékány, I. DRIFT Study of Deuterium-Exchanged Graphite Oxide. *Carbon* **2005**, *43*, 3186.
(49) Kern, R.; Sastrawan, R.; Ferber, J.; Strangl, R.; Luther, J. Modeling and Interpretation of Electrical Impedance Spectra of Dye-Sensitized Solar Cells Operated Under Open-Circuit Conditions. *Electrochim. Acta* **2002**, *47*, 4213−4225.
(50) Han, L.; Koide, N.; Chiba, Y.; Mitate, T. Modeling of an Equivalent Circuit for Dye-Sensitized Solar Cells. *Appl. Phys. Lett.* **2004**, *84*, 2433.
(51) Wang, Q.; Ito, S.; Grätzel, M.; Fabregat-Santiago, F.; Mora-Seró, I.; Bisquert, J.; Bessho, T.; Imai, H. Characteristics of High Efficiency Dye-Sensitized Solar Cells. *J. Phys. Chem. B* **2006**, *110*, 25210−25221.
(52) Orazem, M. E.; Tribollet, B. *Electrochemical Impedance Spectroscopy*; John Wiley & Sons, Inc.: Hoboken, NJ, 2008; Vol. *81*, pp 311−318.

DOI: 10.1021/acsami.5b01938
ACS Appl. Mater. Interfaces 2015, 7, 10863−10871